Supplementary Information for

Layered-material WS_2/topological insulator Bi_2Te_3 heterostructure photodetector with ultrahigh responsivity in the range from 370 to 1550 nm

Jiandong Yao, Zhaoqiang Zheng & Guowei Yang *

State Key Laboratory of Optoelectronic Materials and Technologies, Nanotechnology Research Center, School of Materials Science & Engineering, Sun Yat-sen University, Guangzhou 510275, Guangdong, P. R. China.

*Corresponding author: stsygw@mail.sysu.edu.cn

S1. The (002) diffraction peaks of WS_2 grown on Bi_2Te_3 with different thickness and their full width at half maximum (FWHM).

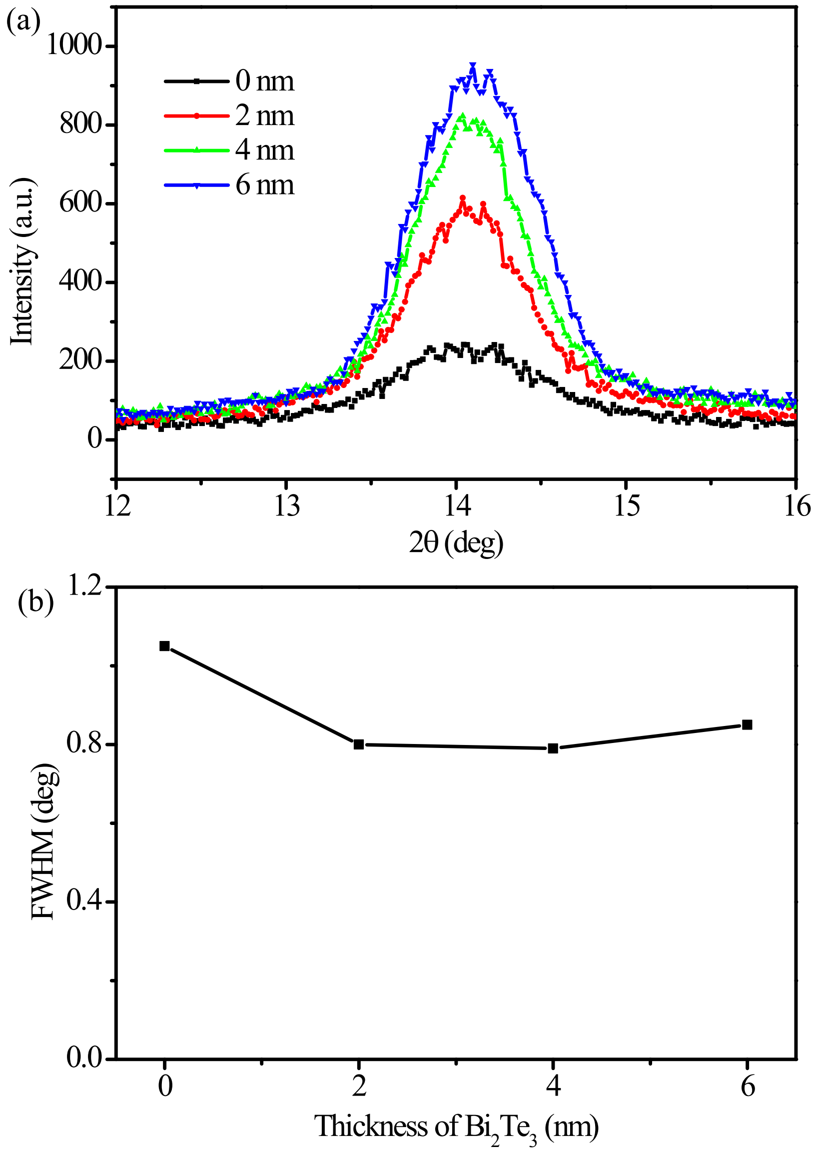

Figure S1. (a) The (002) diffraction peaks of WS_2 grown on Bi_2Te_3 with different thickness and their (b) FWHM. Thickness of WS_2: 15 nm.

S2. AFM thickness profiles of PLD grown WS_2 and Bi_2Te_3.

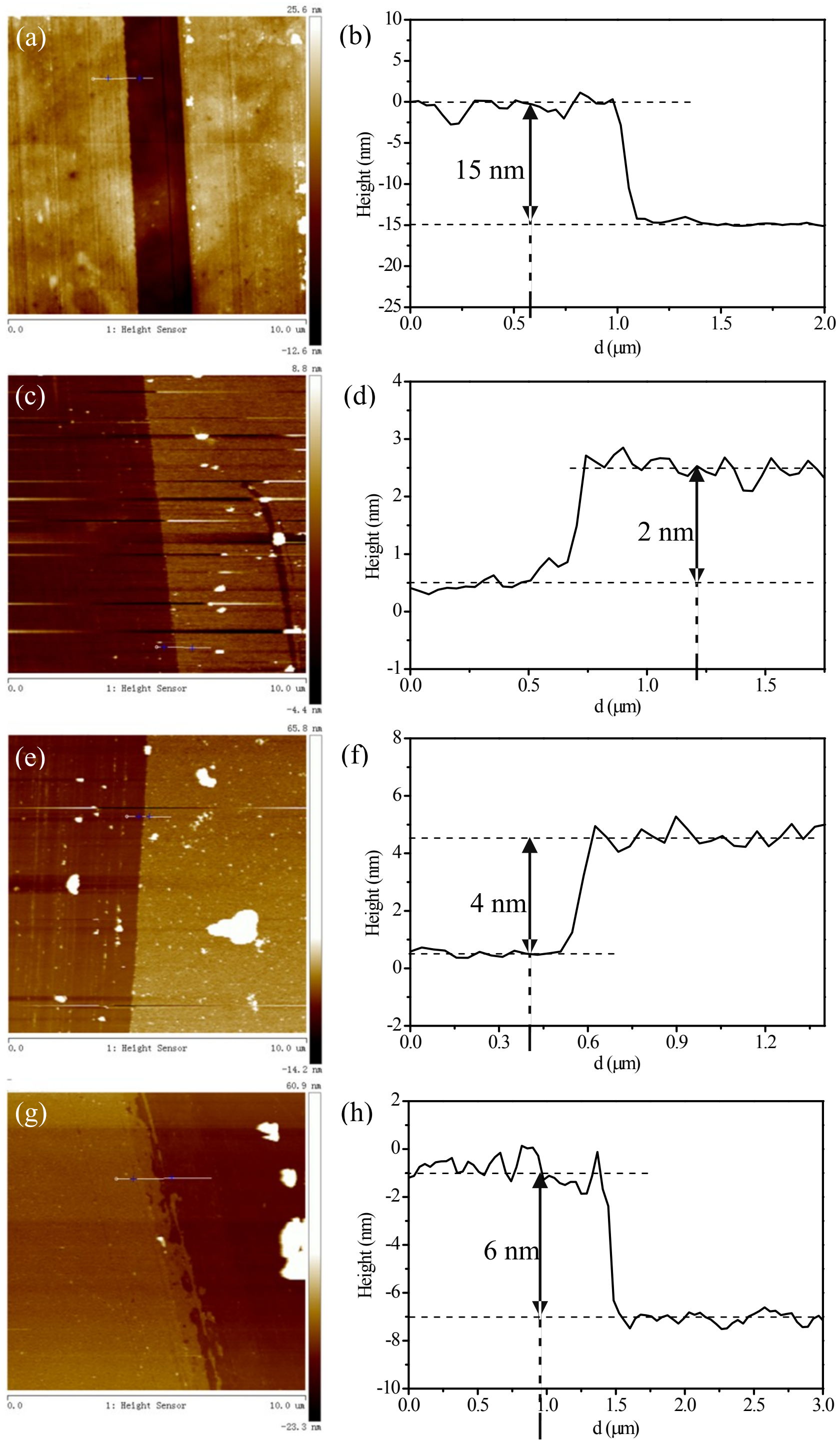

Figure S2. AFM images of PLD-grown (a) WS_2 specimen of 10000 pulse and Bi_2Te_3 specimen of (a) 26, (b) 52 and (c) 78 pulse.

S3. Long-term stability of the WS_2/Bi_2Te_3 photodetectors

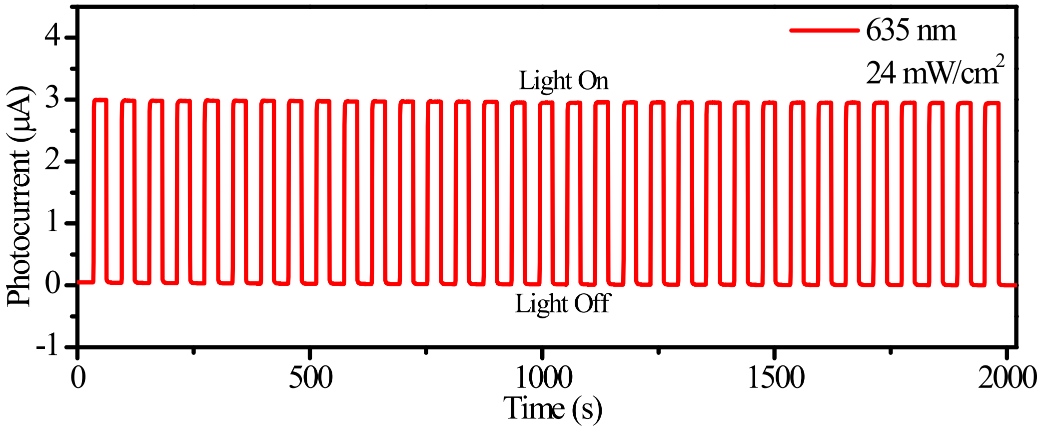

Figure S3. Photoswitching curve of the WS_2/Bi_2Te_3 photodetector in response to long-term periodic 635-nm illumination (~ 2000 s, 33 cycles).

S4. Absorption spectrum of the pure WS_2 film and WS_2/Bi_2Te_3 heterojunction film

Fig. S4 presents the absorption spectrum of the pure WS_2 film (black) and WS_2/Bi_2Te_3 heterojunction film (red). To exclude the absorption from the substrates, transparent mica was exploited as substrates. Note that the periodic oscillation of absorption spectrum comes from the interference effect of the layered mica substrates, which, however, doesn't hinder us from drawing the conclusion. Obviously, absorption edge appears at around 1000 nm for the pure multilayer WS_2 film. After the addition of a Bi_2Te_3 layer, no absorption edge can be observed in the whole measured range extending from 400 to 2000 nm, which is benefit from the small bandgap of Bi_2Te_3 (0.15 eV). Therefore, the above results provide convincing evidence that the photoresponse to the 1550-nm illumination of the WS_2/Bi_2Te_3 heterojunction photodetector originates from the Bi_2Te_3 layer.

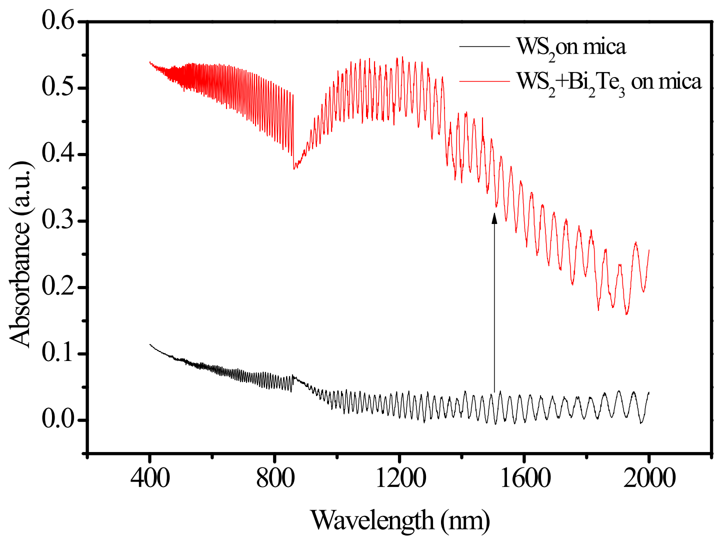

Figure S4. Absorption spectrum of the pure WS_2 film and WS_2/Bi_2Te_3 heterojunction film.

S5. Dark current of the device with different thickness of Bi_2Te_3.

The dark current of the devices with different thickness of Bi_2Te_3 is summarized in Fig. S5. In general, the dark current increases as the thickness of Bi_2Te_3 increases. Note that the dark current of WS_2/Bi_2Te_3 (2 nm) is slightly larger than that of WS_2/Bi_2Te_3 (4 nm), which seems to be counterintuitive. However, it is actually reasonable. When the thickness of Bi_2Te_3 is thinner than ca. 4 nm, the dark current of Bi_2Te_3 is relative smaller on account of its discontinuous nature. Thus, the WS_2 channel dominants the dark current of the WS_2/Bi_2Te_3 photodetector. Since the quality of WS_2 increases as the thickness of Bi_2Te_3 increases, its defect doping thus decreases, resulting in the decrease of the dark current of the WS_2 channel. Thus, the dark current of WS_2/Bi_2Te_3 (2 nm) is slightly larger than that of WS_2/Bi_2Te_3 (4 nm). As the thickness of Bi_2Te_3 increases to 6 nm, it becomes totally continuous and its dark current is much larger than that of WS_2. As a result, the dark current WS_2/Bi_2Te_3 (6 nm) is much larger. Other parameters such as the variation of the contact barrier between the electrode and the channel may also affect, which demands further investigation.

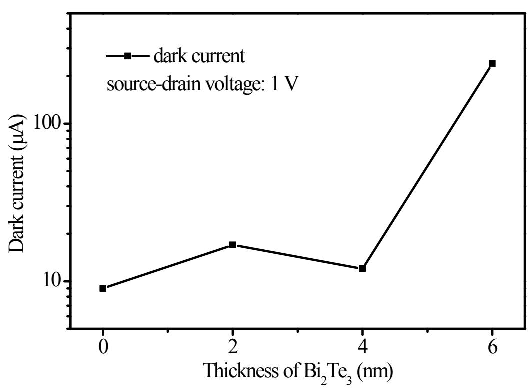

Figure S5. Dark current of the WS_2/Bi_2Te_3 photodetectors.

S6. Application of the interface engineering methodology to PLD-grown MoS_2

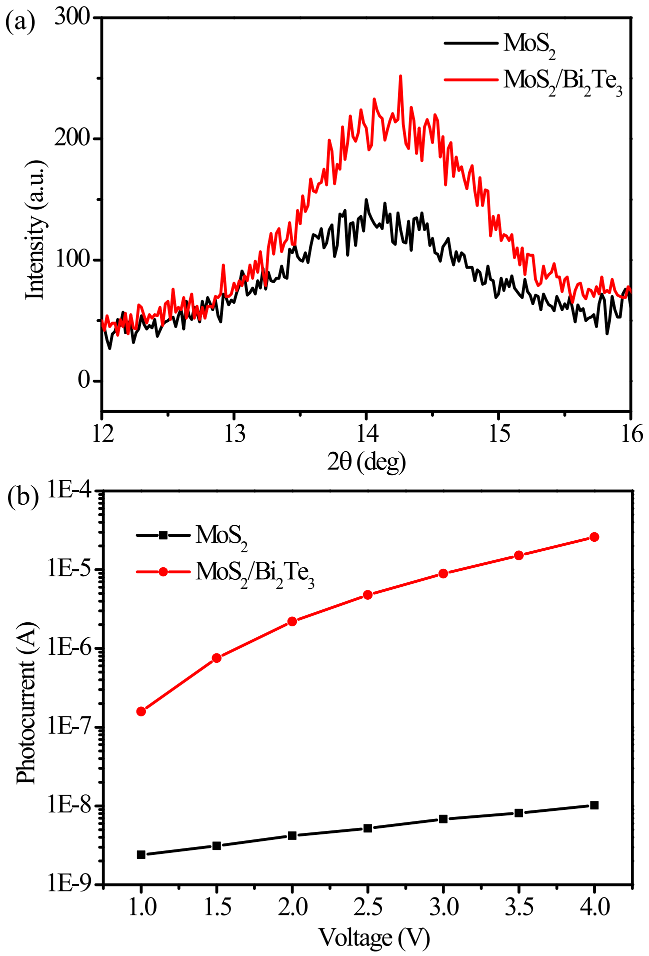

Figure S6. (a) (002) diffraction peaks of the MoS_2 grown on SiO_2 and Bi_2Te_3. (b) Voltage dependent photocurrent of the MoS_2 and MoS_2/Bi_2Te_3 photodetectors.